



Compact binary mergers observed in the first half of the third LIGO-Virgo observing run

LIGO Scientific Collaboration and Virgo Collaboration

Start Time 15:00 UTC

O3a Catalog Paper

dcc.ligo.org/LIGO-P2000061/public

arXiv: [2010.14527](https://arxiv.org/abs/2010.14527)

GWTC-2 Data Release

www.gwopenscience.org/GWTC-2/

Presentation Slides

dcc.ligo.org/G2001898/public

Companion Papers

Populations Webinar 12th November

dcc.ligo.org/LIGO-P2000077/public

arXiv: [2010.14533](https://arxiv.org/abs/2010.14533)

Tests of GR Webinar 19th November

dcc.ligo.org/LIGO-P2000091/public

arXiv: [2010.14529](https://arxiv.org/abs/2010.14529)



Panelists

Ilaria Nardecchia: *Instrument Science*



Derek Davis: *Observing Run 3*

Sarah Caudill: *Search and Detections*



Zoheyr Doctor: *Source Properties*

John Veitch: *Moderator*

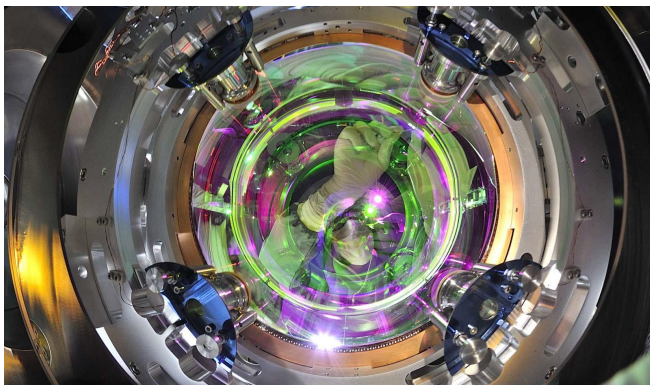


Advanced LIGO and Advanced Virgo

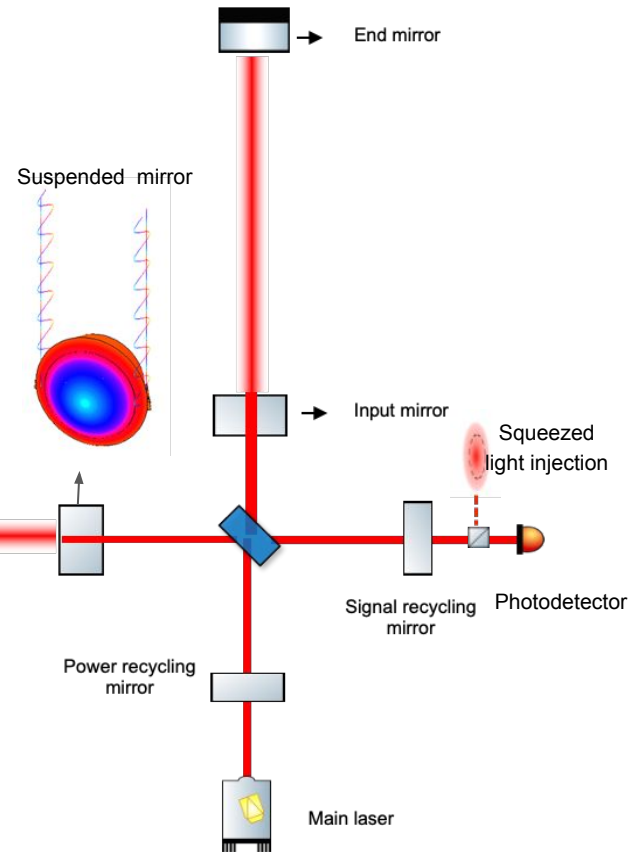
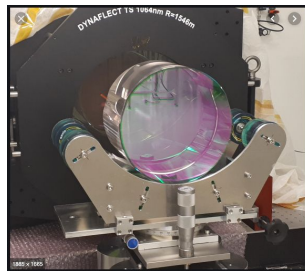
Ilaria Nardecchia

Gravitational wave interferometers

- Best gravitational-wave hunter in the range 10Hz-10kHz;
- Michelson interferometer operating at the dark fringe;
- Fabry-Perot optical cavities in the arms;
- Fabry-Perot core optics:
 - Spherical mirrors
 - High-purity fused silica (diameter 35 cm, mass ~ 40 kg)
 - Suspended by four fibers ~400 μm thick

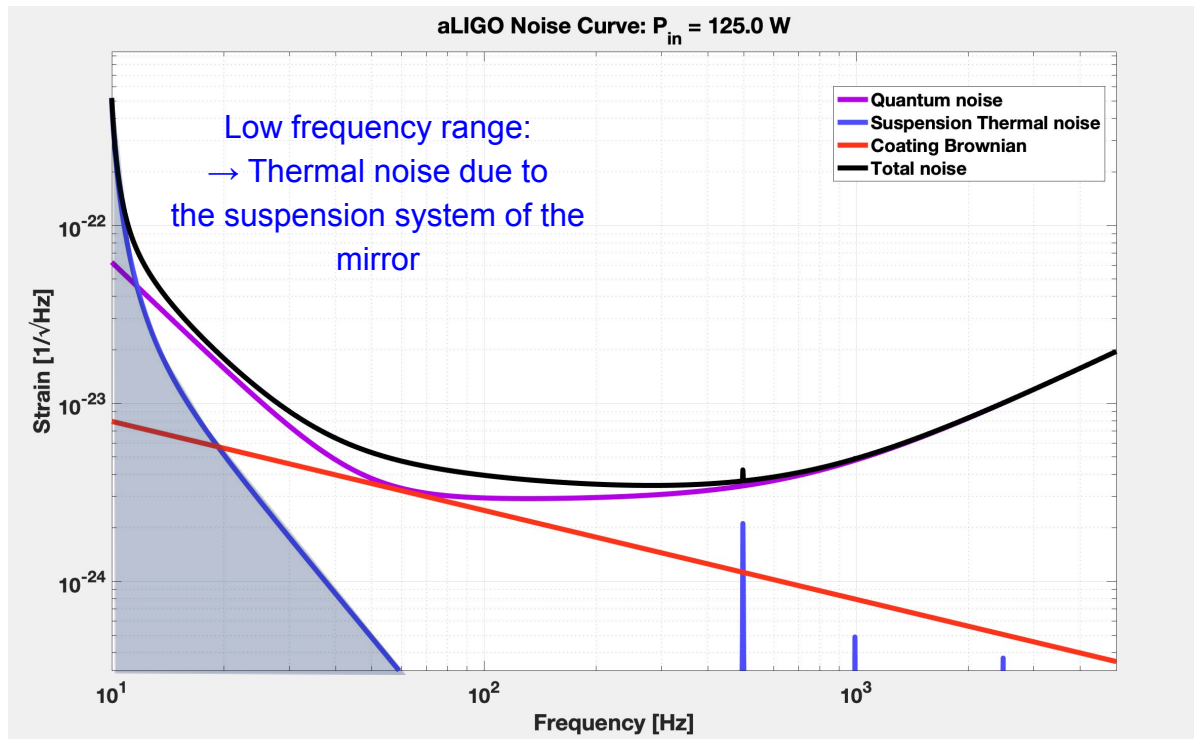
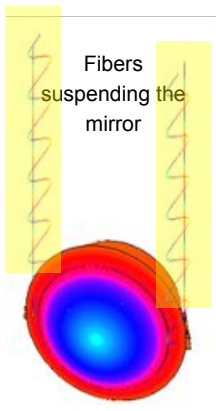


LIGO-Virgo Webinar 2020-11-05

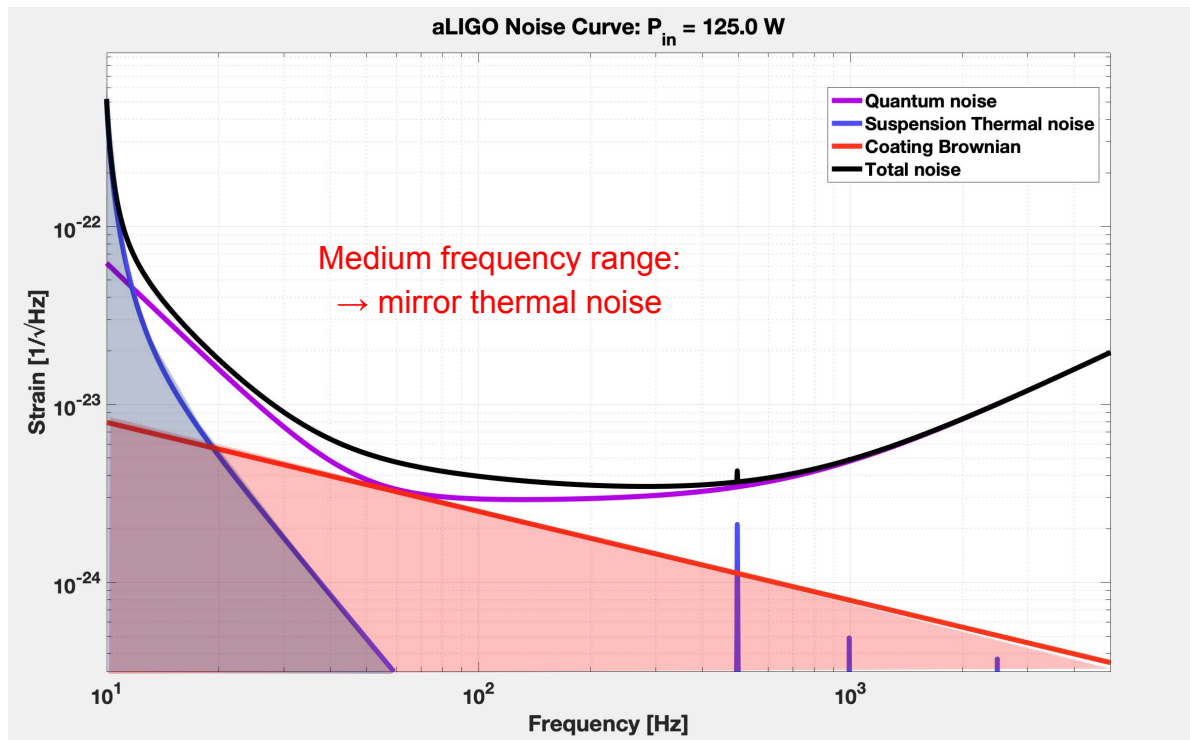
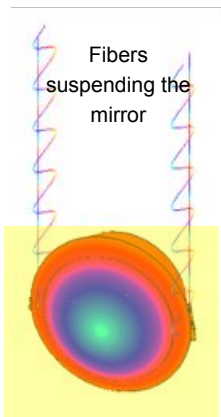


Sensitivity curve

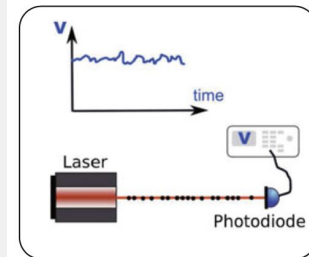
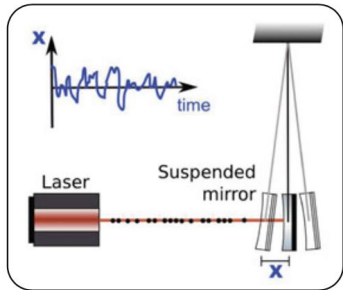
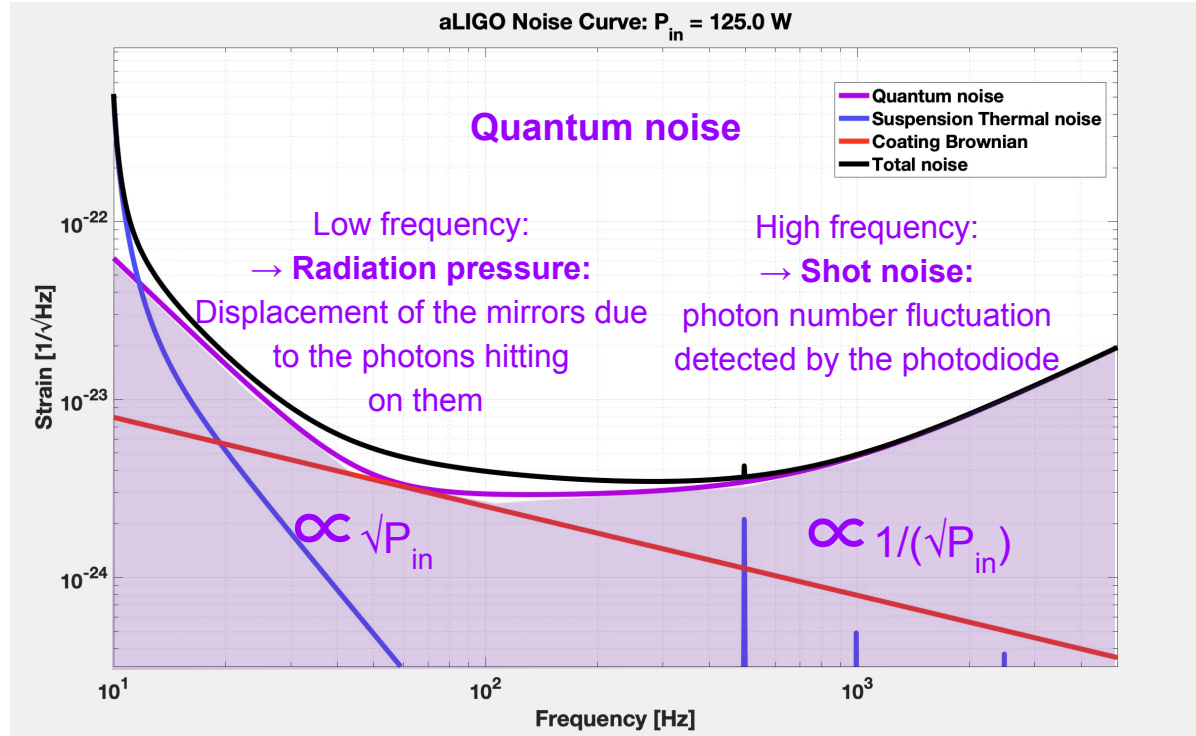
Each detector is characterized by its sensitivity curve



Sensitivity curve



Sensitivity curve

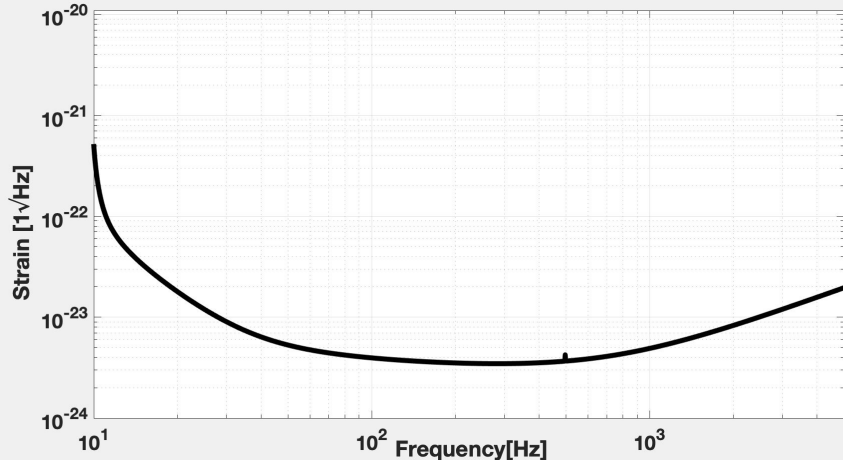




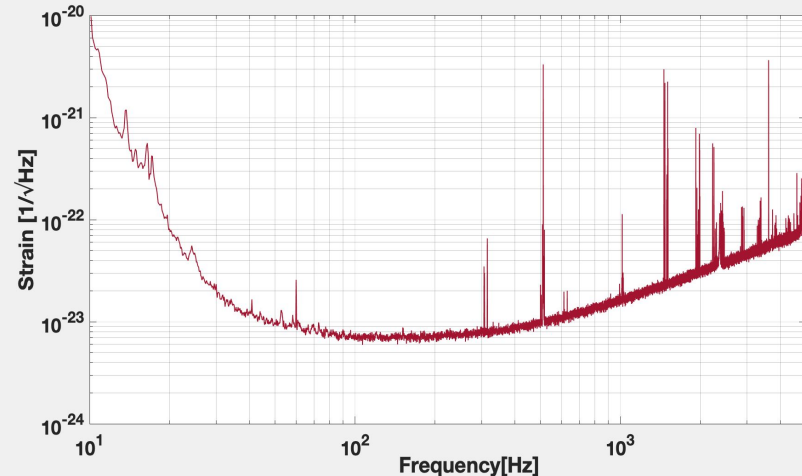
Sensitivity curve

The sensitivity curve indicates the minimum detectable gravitational wave signal

Design



Measured





GW detectors' network (so far)

LIGO Hanford
(Washington, USA)



LIGO Livingston
(Louisiana, USA)



Virgo
(Pisa, Italy)

From O2 to O3a: LIGO Livingston

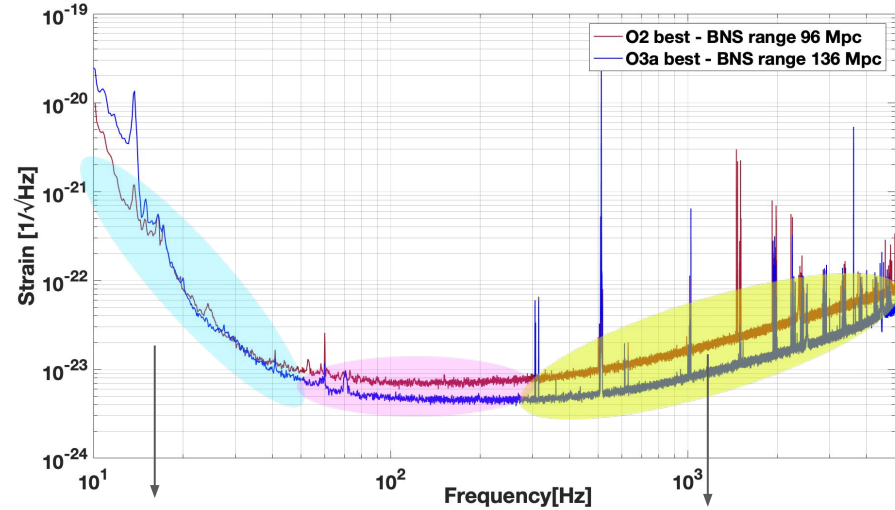
At low frequency:

- Residual noise is still a mystery. Hypothesis: static charge of the mirrors
 - Discharging system installed.
 - Excluded by further investigation.

At medium and high frequency:

Reduce the quantum noise:

- By increasing the circulating power in the detector:
 - input power increased: 25 W \rightarrow 40 W;
 - end test masses with lower scattering losses installed;
- By injecting squeezed light in the detector.



Inspection of one mirror



Optical system producing squeezed light to be injected in the detector

From O2 to O3a: LIGO Hanford

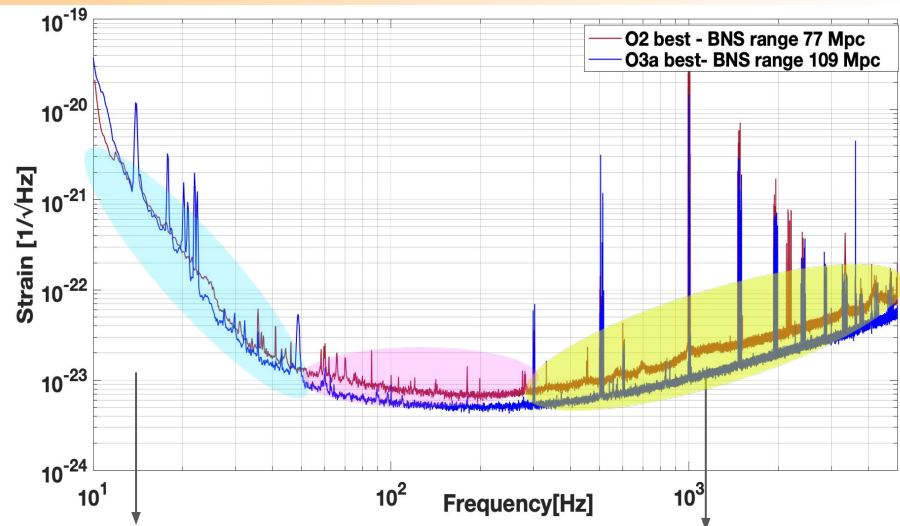
At low frequency:

- Residual noise is still a mystery. Hypothesis: static charge of the mirrors
 - Discharging system installed
 - Excluded by further investigation.

At medium and high frequency:

Reduce the quantum noise:

- By increasing the circulating power in the detector:
 - input power increased: 30 W \rightarrow 37 W;
 - end test masses with lower scattering losses installed;
 - Input test mass with the worst imperfection replaced.
- By injecting squeezed light in the detector.



End mirror discharging system



Optical system producing squeezed light to be injected in the detector

From O2 to O3a: Virgo

At low frequency:

Reduce the thermal noise:

- By installing the fused silica suspensions:
 - Vacuum system upgrades to reduce dust contamination risk

At medium frequency:

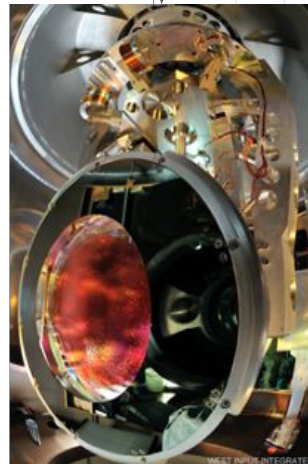
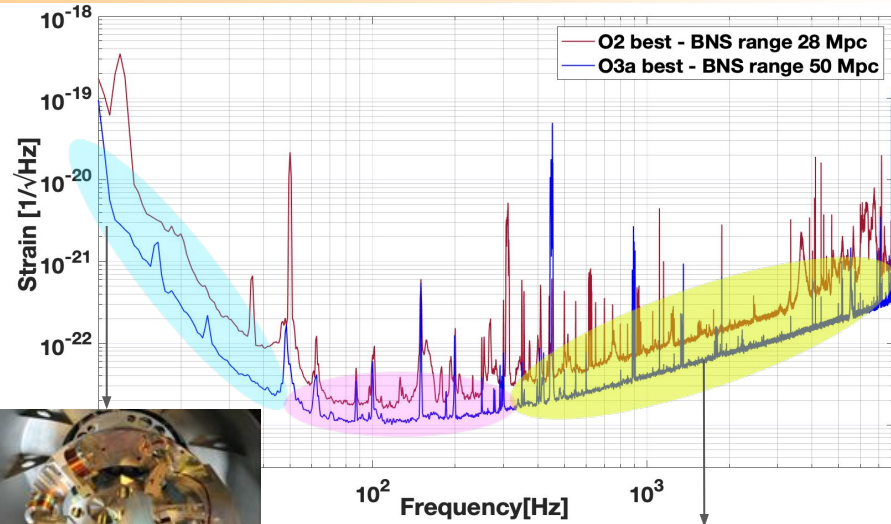
Reduce the electronic noise:

- By installing high quantum efficiency photodiodes

At high frequency:

Reduce the quantum noise:

- By increasing the circulating power in the detector:
 - input power increased: 10 W \rightarrow 20 W;
- By injecting squeezed light in the detector.

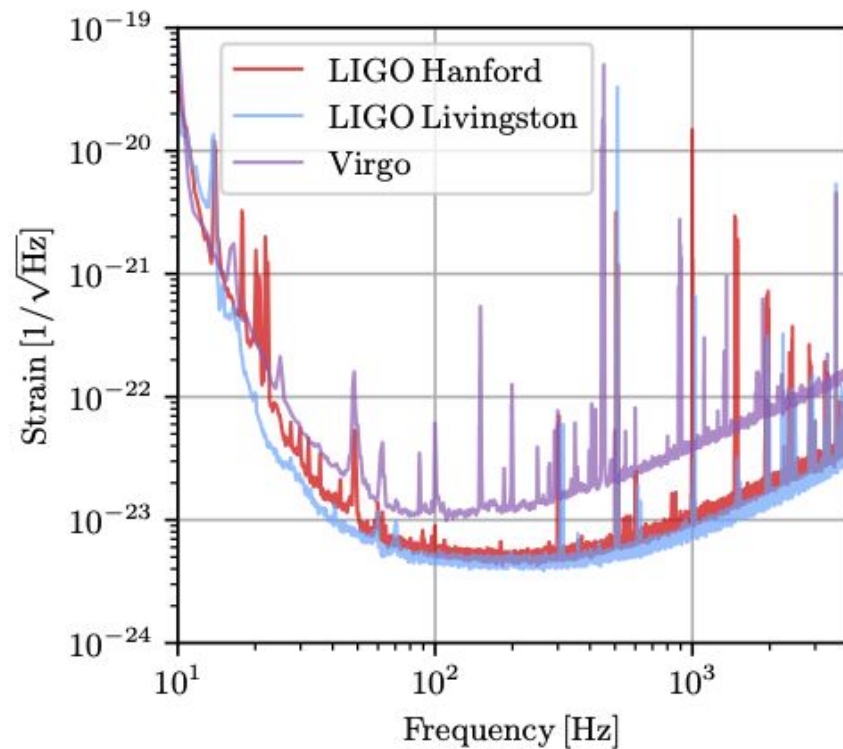


13 *Suspended mirror*



Optical system producing squeezed light to be injected in the detector

LIGO DCC G2001898

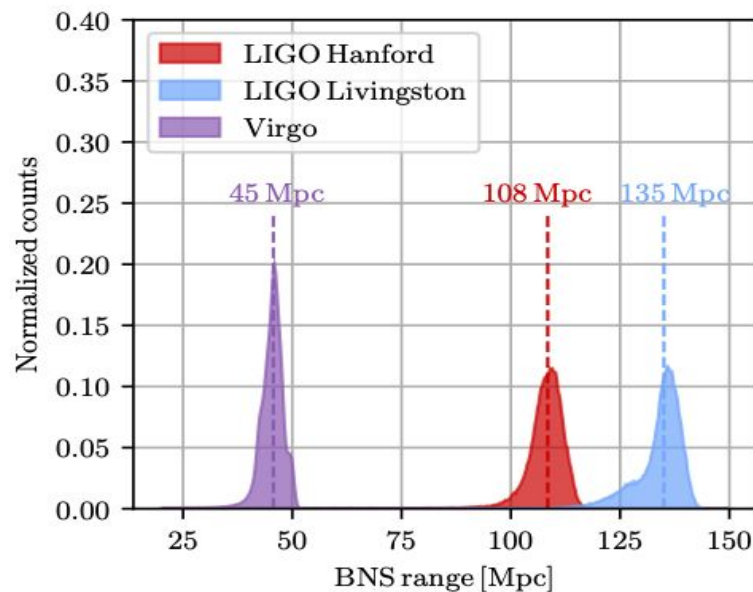
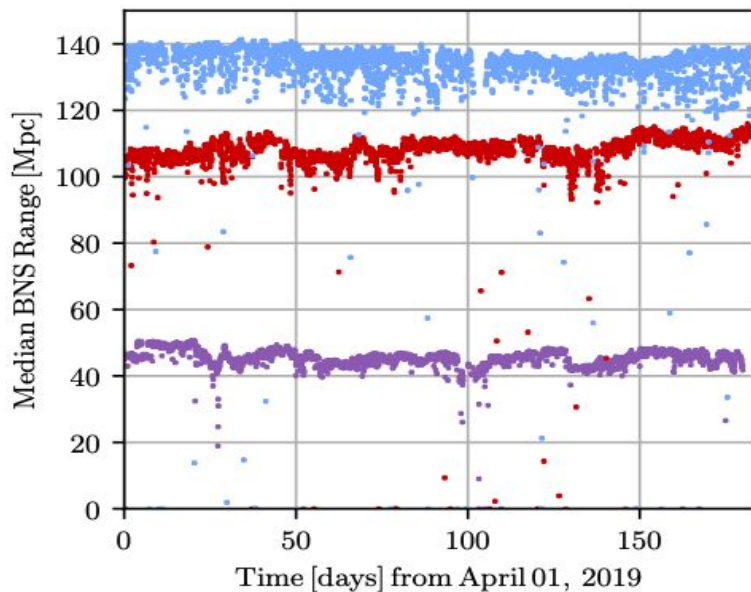


Operations and Data Taking

Derek Davis

Detector Sensitivity during O3a

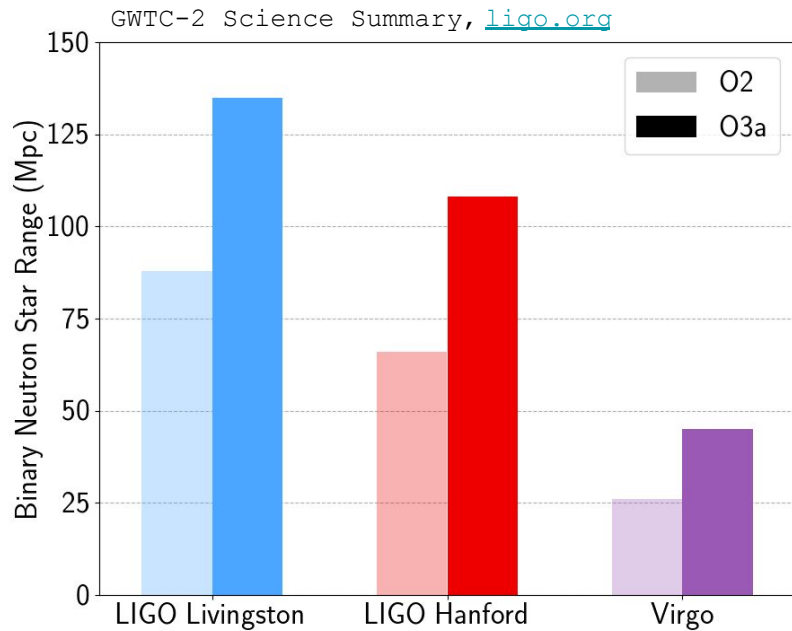
Binary Neutron Star Range: The average distance that GWs from a binary neutron star merger could be observed at a signal-to-noise ratio of 8



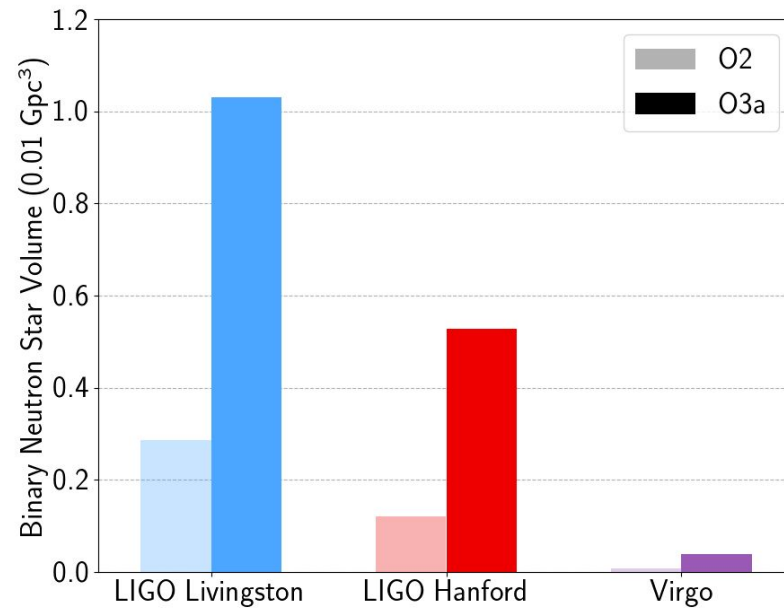
LVC Catalog paper, arXiv: [2010.14527](https://arxiv.org/abs/2010.14527)



O2 vs O3a Sensitivity Comparisons



Sensitive distance



Sensitive volume

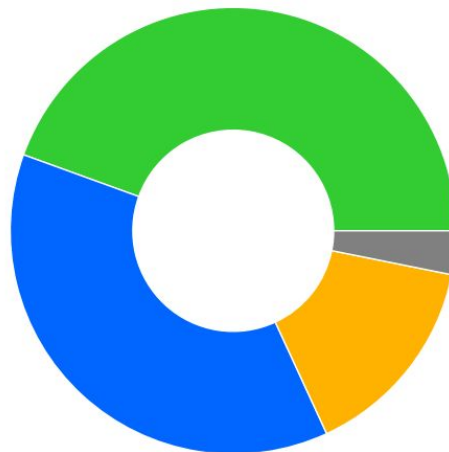
Detector Duty Factor and Uptime

Duty factor: Percentage of wall-clock time that each detector is observing

Uptime: Total amount of time that each detector is observing

<u>O3a</u>	<u>Duty factor</u>	<u>Uptime</u>
Hanford:	71%	130 d
Livingston:	76%	139 d
Virgo:	76%	140 d

<u>O2</u>	<u>Duty factor</u>	<u>Uptime</u>
Hanford:	62%	157 d
Livingston:	61%	155 d
Virgo:	80%	20 d



Network duty factor

[1238166018-1253977218]

- Triple interferometer [44.5%]
- Double interferometer [37.4%]
- Single interferometer [15.0%]
- No interferometer [3.2%]

gw-openscience.org

O3a network duty factor

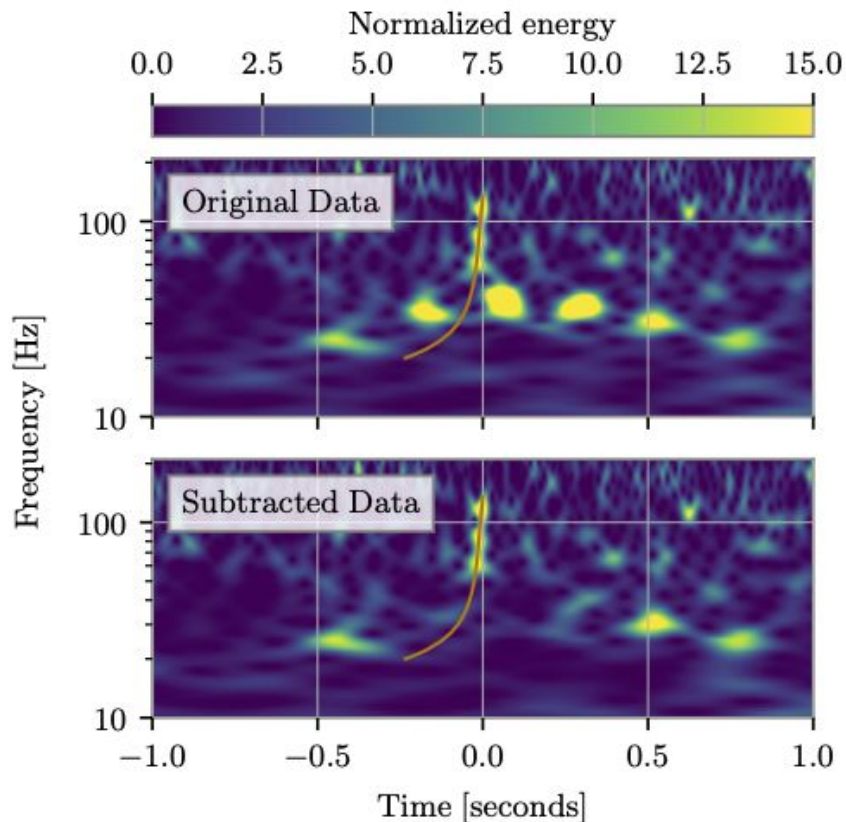
Data Quality Issues in GW Detectors

Glitches: Short duration instrumental artifacts that add excess noise to the interferometer strain data

Common sources of glitches include:

- Scattered laser light
- Thunder claps
- Earthquakes

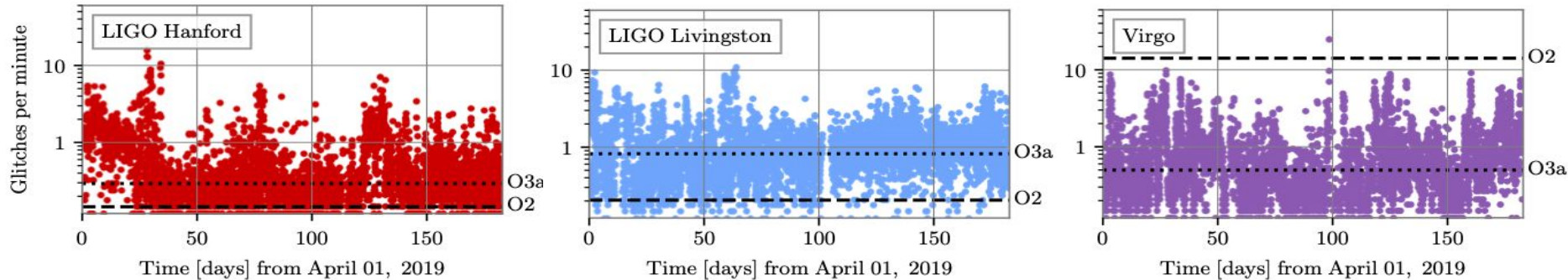
When possible, we subtract glitches with the [BayesWave](#) algorithm near GW candidates for parameter estimation





Rate of Glitches in each Detector

LVC Catalog paper, arXiv: [2010.14527](https://arxiv.org/abs/2010.14527)



During O3a, the median rate of glitches is *higher* than in O2 at LIGO Livingston and LIGO Hanford, and *lower* than in O2 at Virgo

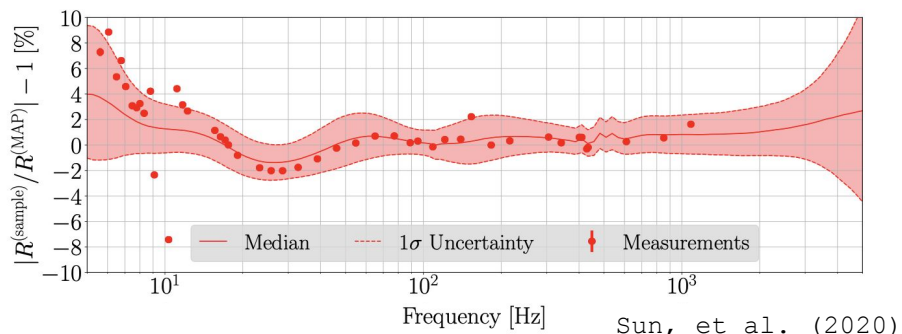
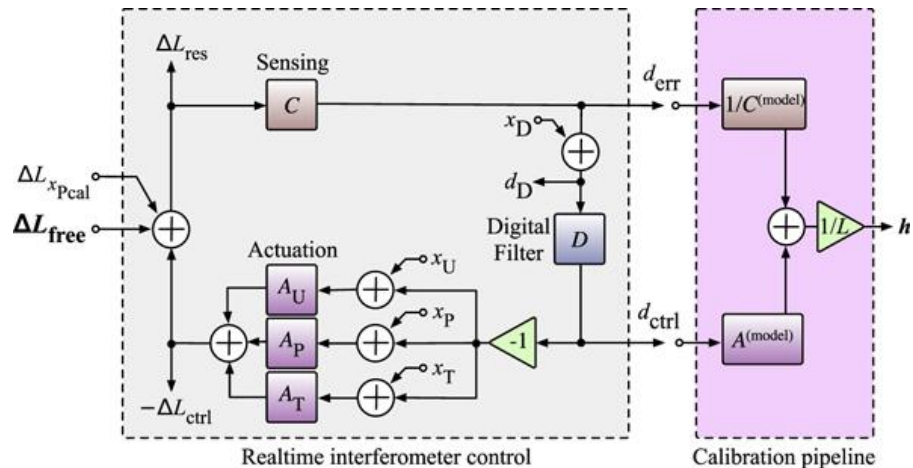
The rate of glitches varies across the observing run due to changing environmental factors and improvements to the detectors to address known sources of glitches

Interferometer Calibration

The interferometers are modeled and calibrated based on the response of the interferometer (*sensing*) and the force applied to the test masses to keep the interferometer stable (*actuation*)

A *photon calibrator*, a laser that pushes on the test masses with a known force, is used as an absolute reference

Measurements of the detector are used to model the systematic uncertainty



Search and Detection

Sarah Caudill

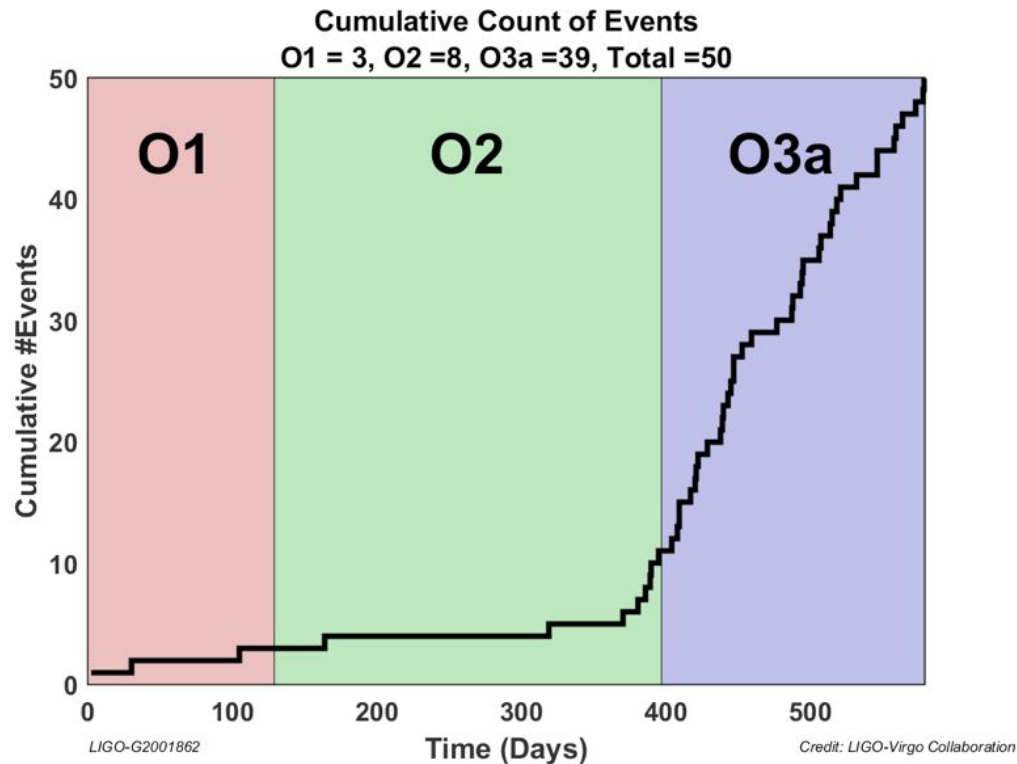


O3a Event Rate

We witnessed a steep increase in event rate in O3a compared to O2.

This is mainly due to the hard work between O2 and O3 to upgrade the LIGO and Virgo detectors.

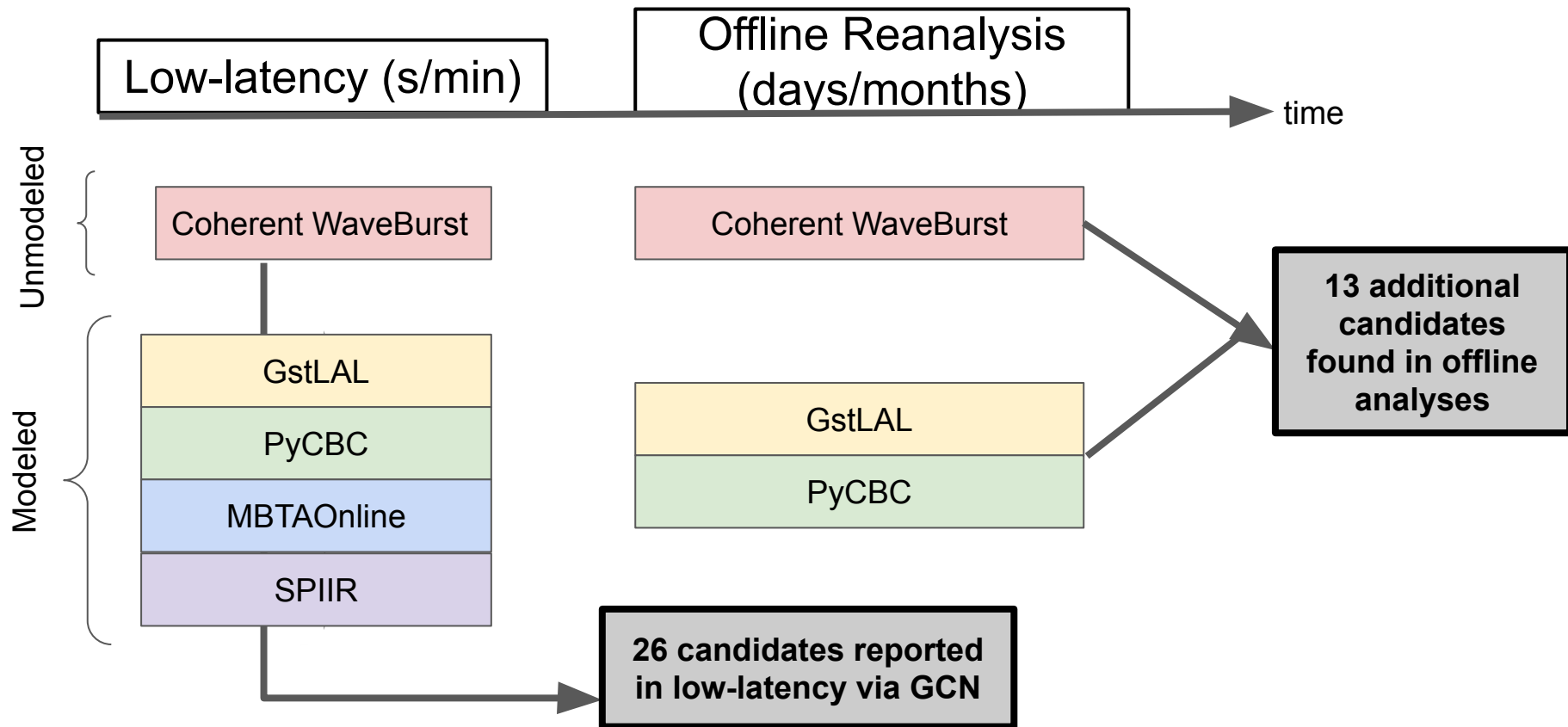
Given the increased sensitivity, the detection of 39 candidates in ~26 weeks of O3a is consistent with GWTC-1.



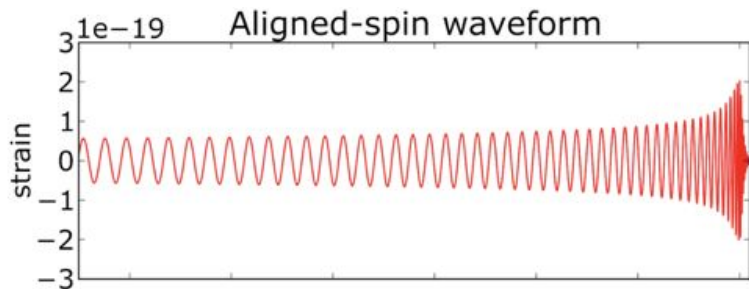
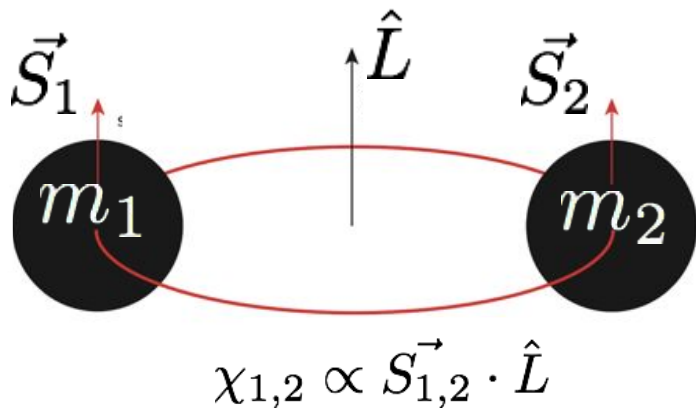
LVC Catalog paper, arXiv: [2010.14527](https://arxiv.org/abs/2010.14527)



Detection Pipelines



Modeled Searches



Offline results from two matched-filter searches are included: GstLAL & PyCBC

Template bank for GstLAL

- m_1, m_2 : 1 - 400 solar masses
- m_{total} : 2 - 758 solar masses
- (Anti-) aligned spin

Template bank for PyCBC

- $m_1 > 1$ solar mass
- $m_{\text{total}} < 500$ solar masses
- mass ratio < 98
- (Anti-) aligned spin

Unmodeled Searches

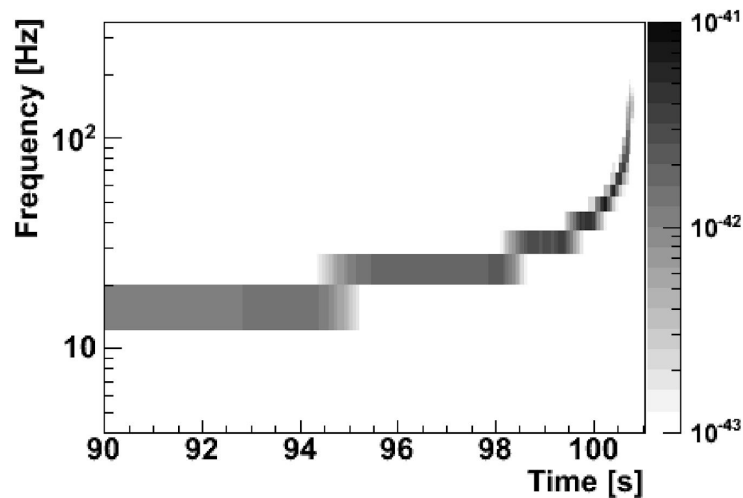
Offline results from one unmodeled search are included: Coherent WaveBurst

Search for transient GW signals without a specific waveform model.

Sensitive to stellar mass BBHs with high chirp masses but not low chirp mass events.

Search requires coincidence between at least 2 detectors.

Wilson-Daubechies-Meyer wavelet transform used by Coherent WaveBurst



Necula, et al. [Journal of Physics](#) (2011)



Search Pipelines

Beyond the initial trigger, search pipelines also rely on:

- Detector coincidence and time delay
- Signal and noise morphology
- Characterization of data quality
- Multivariate ranking statistics

Not only are the detectors better, the search algorithms are better too:

- GstLAL analysis of single, double and triple detector candidates
- Improvements to GstLAL ranking statistic
- PyCBC BBH-focused search with improved ranking statistic



Significance Estimation

Events in GWTC-2 passed the false alarm rate (FAR) threshold of **2 per year**. This means we could have ~3 false alarms mixed in our event list.

To guide us, we include statistical measures of the false alarm rate and probability of BBH astrophysical origin.

$$\text{FAR} = \frac{N(\Lambda \geq \Lambda^*)}{T_{\text{bkgd}}}$$

Number N of background events with ranking statistic Λ higher than Λ^*

p_{astro} - for events consistent with BBH from Poisson mixture model formalism

Farr, et al. (2015)



GW Event Summary

Table IV contains candidates with FAR < 2 per year. Unlike GWTC-1, a p_{astro} cut was not applied.

Candidate events highlighted in red are the most likely to be noise.

Bold candidates were not previously reported.

All significant candidates except GW190425 can be classified as BBH, although GW190814 has some ambiguity.

Candidate events highlighted in yellow were found in only one detector. Thus they have larger uncertainties in the FAR.

Name	Inst.	cWB		GstLAL			PyCBC			PyCBC BBH		
		FAR (yr ⁻¹)	SNR*	FAR (yr ⁻¹)	SNR	p_{astro}	FAR (yr ⁻¹)	SNR*	p_{astro}	FAR (yr ⁻¹)	SNR*	p_{astro}
GW190408.181802	HLV	< 9.5 × 10 ⁻⁴	14.8	< 1.0 × 10 ⁻⁵	14.7	1.00	< 2.5 × 10 ⁻⁵	13.5	1.00	< 7.9 × 10 ⁻⁵	13.6	1.00
GW190412	HLV	< 9.5 × 10 ⁻⁴	19.7	< 1.0 × 10 ⁻⁵	18.9	1.00	< 3.1 × 10 ⁻⁵	17.9	1.00	< 7.9 × 10 ⁻⁵	17.8	1.00
GW190413.052954	HLV	-	-	-	-	-	-	-	-	7.2 × 10 ⁻²	8.6	0.98
GW190413.134308	HLV	-	-	3.8 × 10 ⁻¹	10.0	0.95	-	-	-	4.4 × 10 ⁻²	9.0	0.98
GW190421.213856	HL	3.0 × 10 ⁻¹	9.3	7.7 × 10 ⁻⁴	10.6	1.00	1.9 × 10 ⁰	10.2	0.89	6.6 × 10 ⁻³	10.2	1.00
GW190424.180648	L	-	-	7.8 × 10 ⁻¹¹	10.0	0.91	-	-	-	-	-	-
GW190425	LV	-	-	7.5 × 10 ^{-4†}	13.0	-	-	-	-	-	-	-
GW190426.152155	HLV	-	-	1.4 × 10 ⁰	10.1	-	-	-	-	-	-	-
GW190503.185404	HLV	1.8 × 10 ⁻³	11.5	< 1.0 × 10 ⁻⁵	12.1	1.00	3.7 × 10 ⁻²	12.2	1.00	< 7.9 × 10 ⁻⁵	12.2	1.00
GW190512.180714	HLV	8.8 × 10 ⁻¹	10.7	< 1.0 × 10 ⁻⁵	12.3	1.00	3.8 × 10 ⁻⁵	12.2	1.00	< 5.7 × 10 ⁻⁵	12.2	1.00
GW190513.205428	HLV	-	-	< 1.0 × 10 ⁻⁵	12.3	1.00	3.7 × 10 ⁻⁴	11.8	1.00	< 5.7 × 10 ⁻⁵	11.9	1.00
GW190514.065416	HL	-	-	-	-	-	-	-	-	5.3 × 10 ⁻¹	8.3	0.96
GW190517.055101	HLV	6.5 × 10 ⁻³	10.7	9.6 × 10 ⁻⁴	10.6	1.00	1.8 × 10 ⁻²	10.4	1.00	< 5.7 × 10 ⁻⁵	10.2	1.00
GW190519.153544	HLV	3.1 × 10 ⁻⁴	14.0	< 1.0 × 10 ⁻⁵	12.0	1.00	< 1.8 × 10 ⁻⁵	13.0	1.00	< 5.7 × 10 ⁻⁵	13.0	1.00
GW190521	HLV	2.0 × 10 ⁻⁴	14.4	1.2 × 10 ⁻³	14.7	1.00	1.1 × 10 ⁰	12.6	0.93	-	-	-
GW190521.074359	HL	< 1.0 × 10 ⁻⁴	24.7	< 1.0 × 10 ⁻⁵	24.4	1.00	< 1.8 × 10 ⁻⁵	24.0	1.00	< 5.7 × 10 ⁻⁵	24.0	1.00
GW190527.092055	HL	-	-	6.2 × 10 ⁻²	8.9	0.99	-	-	-	-	-	-
GW190602.175927	HLV	1.5 × 10 ⁻²	11.1	1.1 × 10 ⁻⁵	12.1	1.00	-	-	-	1.5 × 10 ⁻²	11.4	1.00
GW190620.030421	LV	-	-	2.9 × 10 ^{-3†}	10.9	1.00	-	-	-	-	-	-
GW190630.185205	LV	-	-	< 1.0 × 10 ⁻⁵	15.6	1.00	-	-	-	-	-	-
GW190701.203306	HLV	5.5 × 10 ⁻¹	10.2	1.1 × 10 ⁻²	11.6	1.00	-	-	-	-	-	-
GW190706.222641	HLV	< 1.0 × 10 ⁻³	12.7	< 1.0 × 10 ⁻⁵	12.3	1.00	6.7 × 10 ⁻⁵	11.7	1.00	< 4.6 × 10 ⁻⁵	12.3	1.00
GW190707.093326	HL	-	-	< 1.0 × 10 ⁻⁵	13.0	1.00	< 1.0 × 10 ⁻⁵	12.8	1.00	< 4.6 × 10 ⁻⁵	12.8	1.00
GW190708.232457	LV	-	-	2.8 × 10 ^{-5†}	13.1	1.00	-	-	-	-	-	-
GW190719.215514	HL	-	-	-	-	-	-	-	-	1.6 × 10 ⁰	8.0	0.82
GW190720.000836	HLV	-	-	< 1.0 × 10 ⁻⁵	11.7	1.00	< 2.0 × 10 ⁻⁵	10.6	1.00	< 3.7 × 10 ⁻⁵	10.5	1.00
GW190727.060333	HLV	8.8 × 10 ⁻²	11.4	< 1.0 × 10 ⁻⁵	12.3	1.00	3.5 × 10 ⁻³	11.5	1.00	< 3.7 × 10 ⁻⁵	11.8	1.00
GW190728.064510	HLV	-	-	< 1.0 × 10 ⁻⁵	13.6	1.00	< 1.6 × 10 ⁻⁵	13.4	1.00	< 3.7 × 10 ⁻⁵	13.4	1.00
GW190731.140936	HL	-	-	2.1 × 10 ⁻¹	8.5	0.97	-	-	-	2.8 × 10 ⁻¹	8.2	0.96
GW190803.022701	HLV	-	-	3.2 × 10 ⁻²	9.0	0.99	-	-	-	2.7 × 10 ⁻²	8.6	0.99
GW190814	LV	-	-	< 1.0 × 10 ⁻⁵	22.2	1.00	-	-	-	-	-	-
GW190828.063405	HLV	< 9.6 × 10 ⁻⁴	16.6	< 1.0 × 10 ⁻⁵	16.0	1.00	< 1.5 × 10 ⁻⁵	15.3	1.00	< 3.3 × 10 ⁻⁵	15.3	1.00
GW190828.065509	HLV	-	-	< 1.0 × 10 ⁻⁵	11.1	1.00	5.8 × 10 ⁻⁵	10.8	1.00	< 3.3 × 10 ⁻⁵	10.8	1.00
GW190909.114149	HL	-	-	1.1 × 10 ⁰	8.5	0.89	-	-	-	-	-	-
GW190910.112807	LV	-	-	1.9 × 10 ^{-5†}	13.4	1.00	-	-	-	-	-	-
GW190915.235702	HLV	< 1.0 × 10 ⁻³	12.3	< 1.0 × 10 ⁻⁵	13.1	1.00	8.6 × 10 ⁻⁴	13.0	1.00	< 3.3 × 10 ⁻⁵	12.7	1.00
GW190924.021846	HLV	-	-	< 1.0 × 10 ⁻⁵	13.2	1.00	< 6.3 × 10 ⁻⁵	12.5	1.00	< 3.3 × 10 ⁻⁵	12.4	1.00
GW190929.012149	HLV	-	-	2.0 × 10 ⁻²	9.9	1.00	-	-	-	-	-	-
GW190930.133541	HL	-	-	5.8 × 10 ⁻¹	10.0	0.92	3.4 × 10 ⁻²	9.7	1.00	3.3 × 10 ⁻²	9.8	0.99

Source Properties

Zoheyr Doctor



Estimation of Source Parameters

$$p(\underbrace{\vec{\vartheta}}_{\text{pink}} | \underbrace{\vec{d}}_{\text{green}}) \propto p(\underbrace{\vec{d}}_{\text{blue}} | \underbrace{\vec{\vartheta}}_{\text{orange}}) \pi(\vec{\vartheta})$$

Source Parameters ϑ : Masses (m_1, m_2) and 3-D dimensionless spin vectors (χ_1, χ_2) of the two coalescing objects, luminosity distance, sky position,...

Data d : Strain in all operating detectors

Likelihood: Gaussian in residuals between strain data and model

Priors: Uniform in detector-frame masses ($[1+z]m_1, [1+z]m_2$, where z is redshift), uniform in dimensionless spin magnitude, isotropic in spin orientations. Distance prior proportional to uniform rate density in comoving frame.



Waveform Models

We perform analyses with multiple waveform models and with different physical effects, e.g. spin precession, higher-mode emission

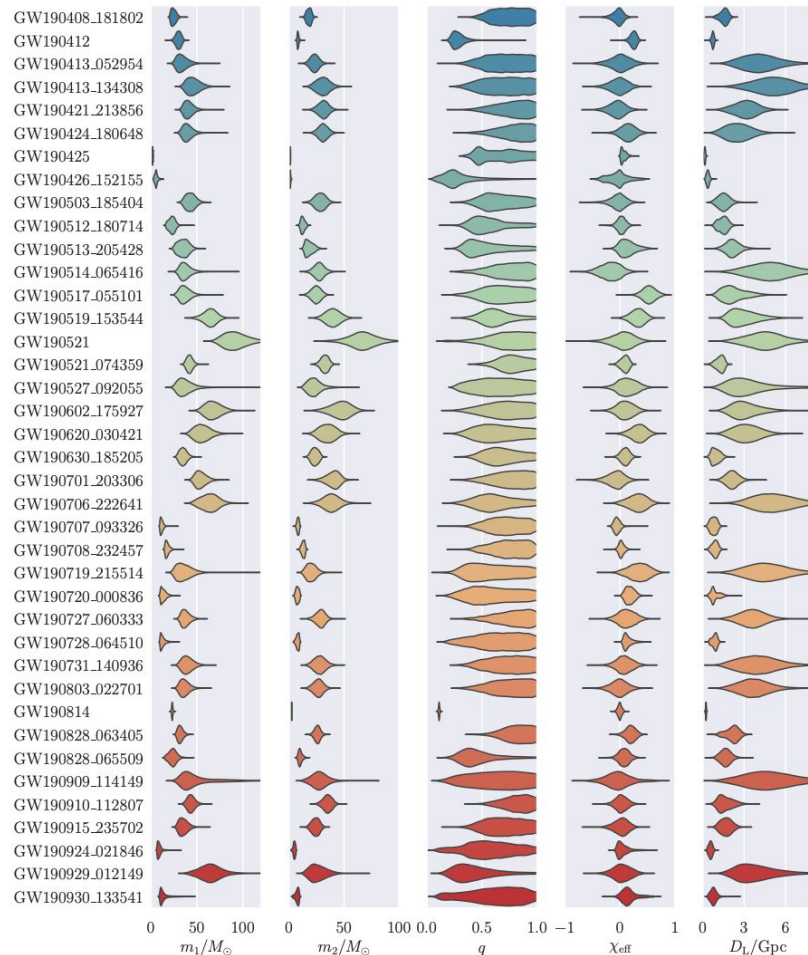
Combined key	Waveform name	Precession	Multipoles ($\ell, m $)
ZeroSpinIMR*	IMRPhenomD	×	(2, 2)
AlignedSpinIMR	SEOBNRv4_ROM	×	(2, 2)
AlignedSpinIMRHM	IMRPhenomHM	×	(2, 2), (2, 1), (3, 3), (3, 2), (4, 4), (4, 3)
	SEOBNRv4HM_ROM	×	(2, 2), (2, 1), (3, 3), (4, 4), (5, 5)
PrecessingSpinIMR	SEOBNRv4P	✓	(2, 2), (2, 1)
	IMRPhenomPv2	✓	(2, 2)
PrecessingSpinIMRHM	IMRPhenomPv3HM	✓	(2, 2), (2, 1), (3, 3), (3, 2), (4, 4), (4, 3)
	NRSur7dq4	✓	$\ell \leq 4$
	SEOBNRv4PHM	✓	(2, 2), (2, 1), (3, 3), (4, 4), (5, 5)
AlignedSpinTidal†	IMRPhenomD_NRTidal	×	(2, 2)
	TEOBResumS	×	(2, 2)
	SEOBNRv4T_surrogate	×	(2, 2)
PrecessingSpinIMRTidal†	IMRPhenomP_NRTidal	✓	(2, 2)
AlignedSpinInspiralTidal†	TaylorF2	×	(2, 2)
AlignedSpinIMRTidal-NSBH	SEOBNRv4_ROM_NRTidalv2_NSBH	×	(2, 2)
	IMRPhenomNSBH	×	(2, 2)

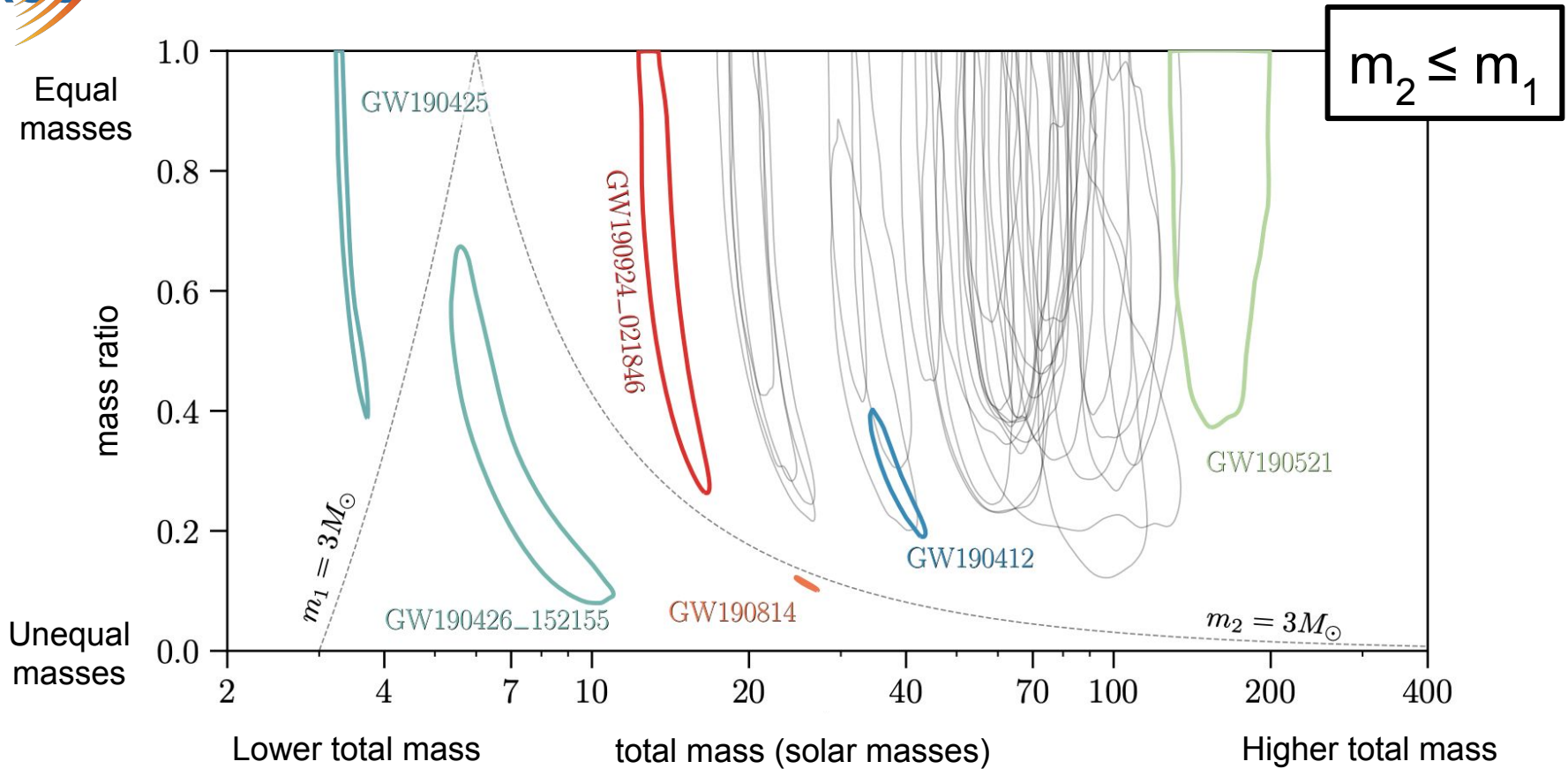
LVC Catalog paper, arXiv: [2010.14527](https://arxiv.org/abs/2010.14527)



Source Parameters

- We make estimates of the source parameters for every event using multiple waveform models.
- LALInference, Bilby, and RIFT samplers used to produce posterior samples.
- Fiducial results are combined posteriors under different waveform models.
- Results using models with $\ell > 2$ modes shown if 1D marginal parameter estimates differ from results without higher modes.
- Posterior samples from all runs are now publicly available.





LVC Catalog paper, arXiv: [2010.14527](https://arxiv.org/abs/2010.14527)

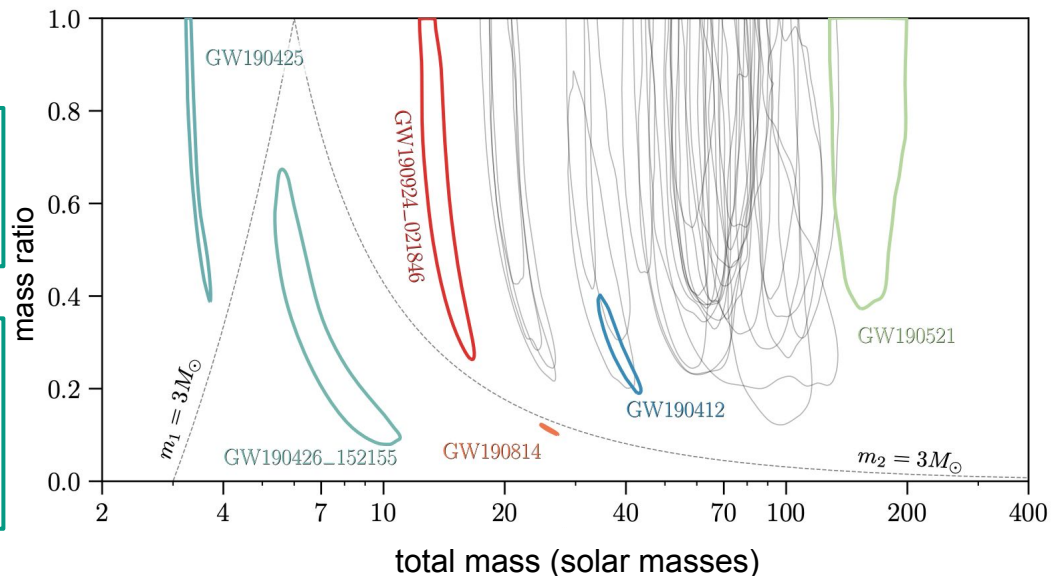


GW190425: Both components of mass $< 3M_{\odot}$. Consistent with binary neutron star merger.

GW190426_152155: Highest FAR event. One component with mass $< 3M_{\odot}$. Parameter estimates consistent with neutron-star-black-hole merger.

GW190924_021846: Of $m_2 > 3M_{\odot}$ systems, lowest total mass system and lowest component mass.

GW190814: $m_2 < 3M_{\odot}$, spin of more massive object constrained to near zero.

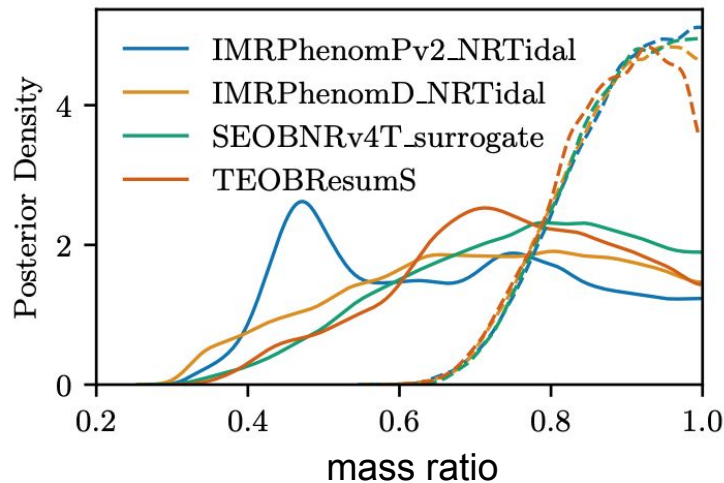
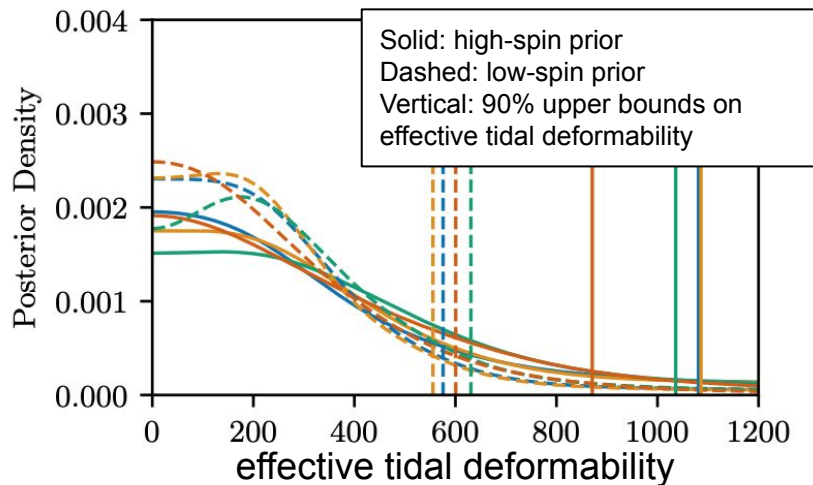


GW190412: confidently unequal mass merger, but not necessarily most unequal mass merger with $m_2 > 3M_{\odot}$ because of broad q posteriors on other events.

GW190521: likely from most massive system and most massive component black hole

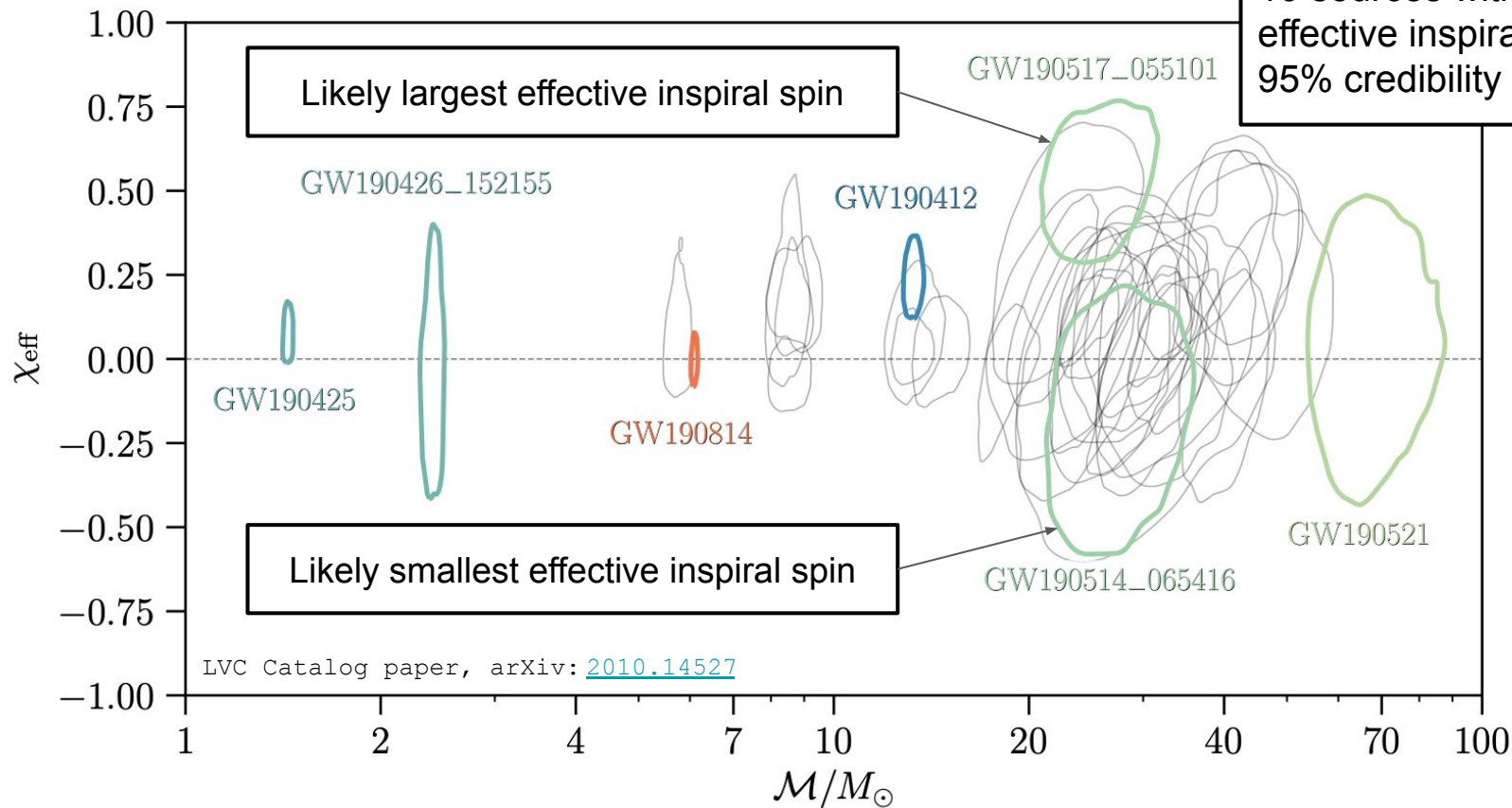


- New parameter estimation results for GW190425 with `TEOBResumS` and `SEOBNRv4T_surrogate` models.
- Consistent results to those previously published with `IMRPhenom` models.
- Slightly tighter constraints on tidal deformability and mass ratio with `EOB` models when allowing for higher spins (solid lines).

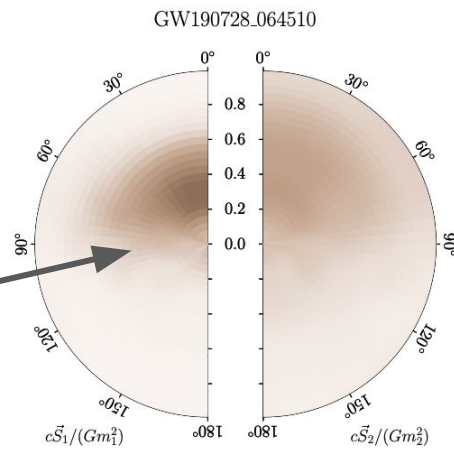
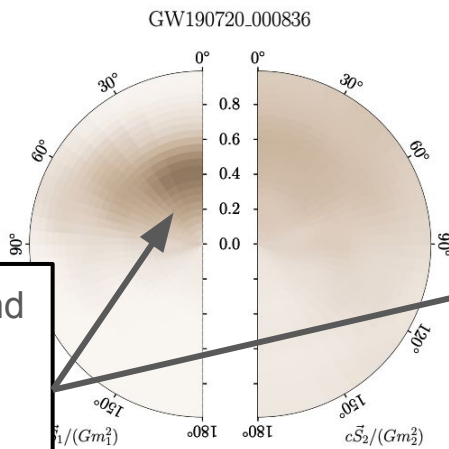
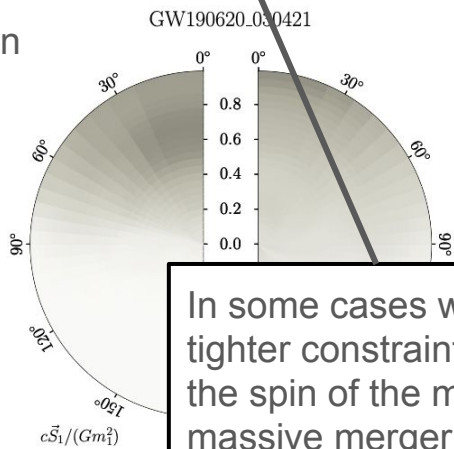
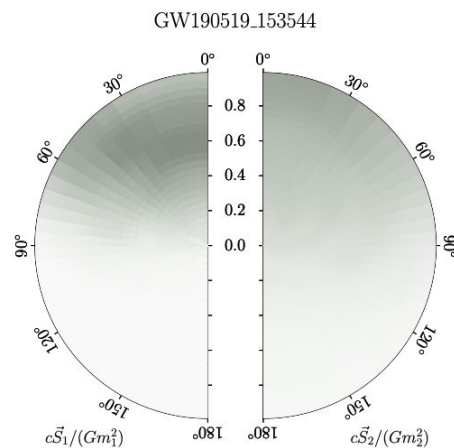
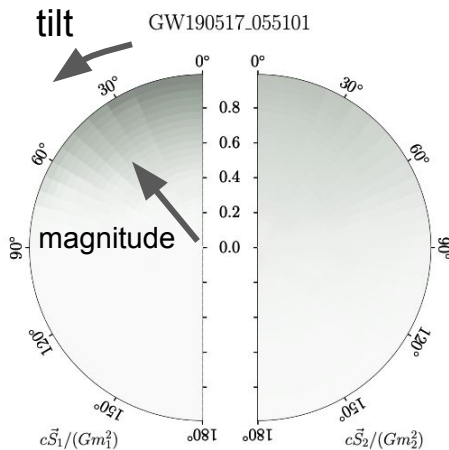
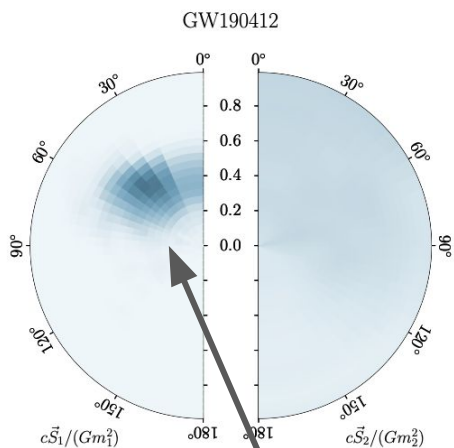




$$\chi_{\text{eff}} = \frac{(m_1 \vec{\chi}_1 + m_2 \vec{\chi}_2) \cdot \hat{L}_N}{M} \quad \mathcal{M} = \frac{(m_1 m_2)^{3/5}}{(m_1 + m_2)^{1/5}}$$



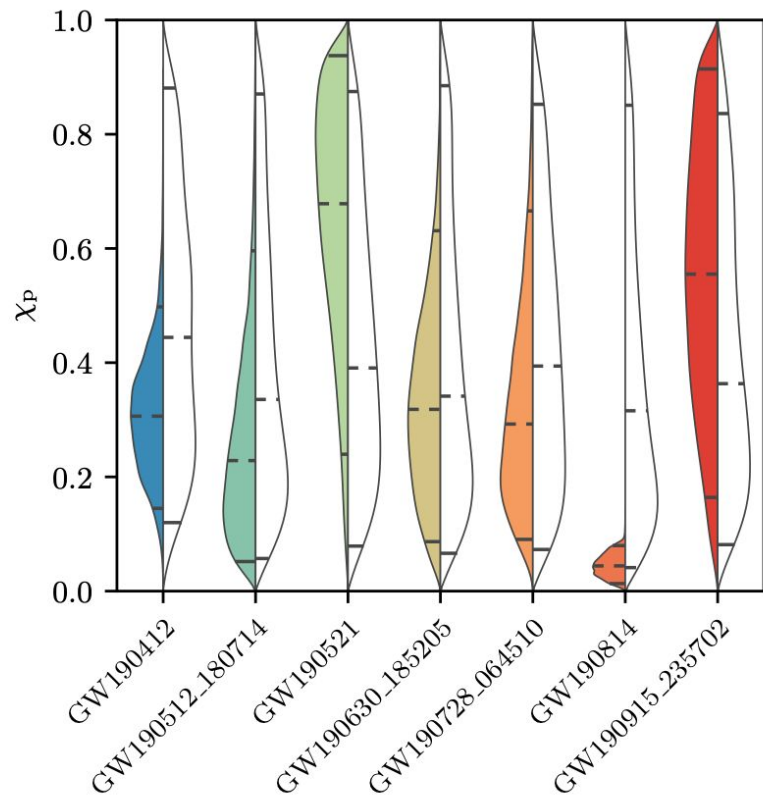
Left (right) halves of the circles are shaded in proportion to posterior on spin magnitude and tilt of the more (less) massive component



In some cases we find tighter constraints on the spin of the more massive merger component.

Precession?

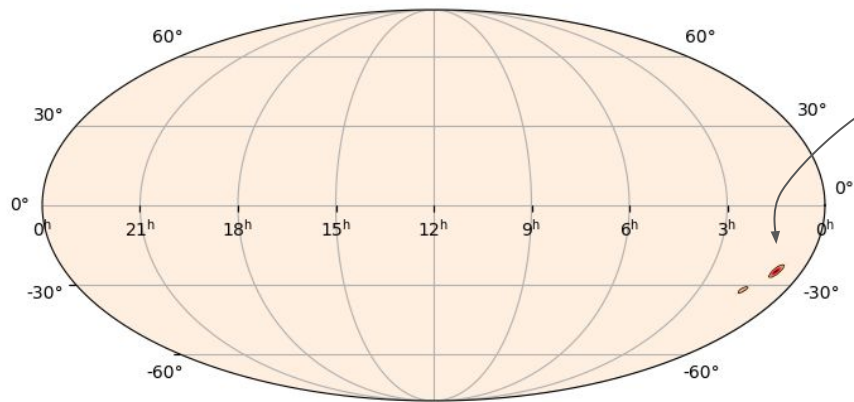
- A few systems where posterior on effective precession spin parameter χ_p (measure of spin in orbital plane) differs from the prior.
- More massive component in source of GW190814 has small spin magnitude, and therefore we infer small effective precession spin parameter.
- Mild evidence for spin precession in sources of GW190412 and GW190521.
- No systems with strong evidence of precession with the models considered in this work.



LVC Catalog paper, arXiv: [2010.14527](https://arxiv.org/abs/2010.14527)

3D Sky Localizations

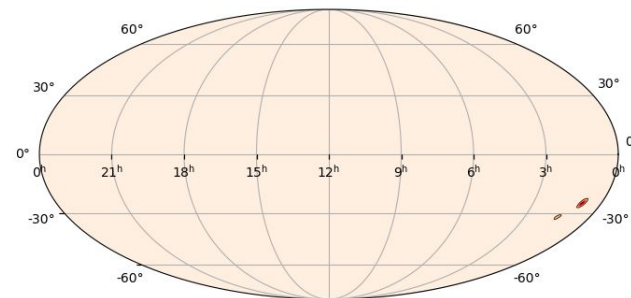
- A few O3a GWs from much large distances than seen in O1/O2!
 - Sources of GW190413_134308, GW190514_065416, GW190521, GW190706_222641, GW190719_215514, and GW190909_114149 have estimated luminosity distances of ~ 5 Gpc ($z \sim 0.75$).



- GW190814 is the best localized event:
 - Localized on sky to 19 sq. deg. (90% credible region)
 - Localized to co-moving volume of 3.2×10^{-5} Gpc³ (90% credible region)

3D Sky Localizations

- A few O3a GWs from much large distances than seen in O1/O2!
 - Sources of GW190413_134308, GW190514_065416, GW190521, GW190706_222641, GW190719_215514, and GW190909_114149 have estimated luminosity distances of ~ 5 Gpc ($z \sim 0.75$).
- GW190814 is the best localized event:
 - Localized on sky to 19 sq. deg. (90% credible region)
 - Localized to co-moving volume of 3.2×10^{-5} Gpc³ (90%)
- GW190424_180648 is the worst localized event:
 - 26,000 sq. deg. credible sky area, 31 Gpc³ localization volume



Outlook

John Veitch



Astrophysical Implications

Population-level analyses of all-GWTC-2 reveals

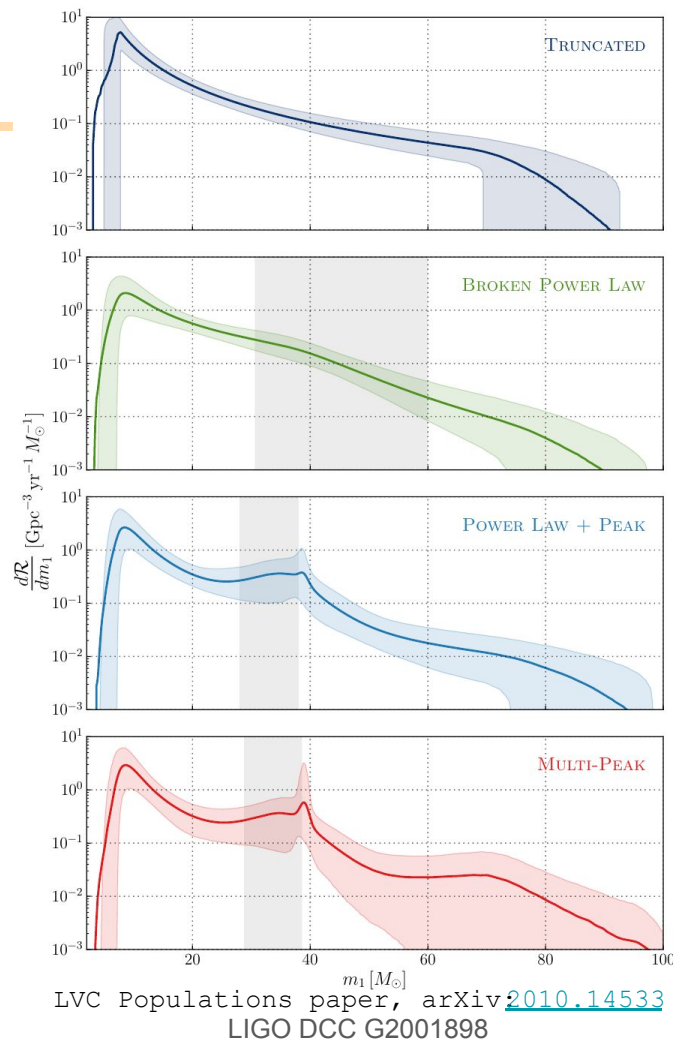
- BBH merger rate $\mathcal{R}_{\text{BBH}} = 23.9_{-8.6}^{+14.9} \text{ Gpc}^{-3} \text{ yr}^{-1}$
- BNS merger rate $\mathcal{R}_{\text{BNS}} = 320_{-240}^{+490} \text{ Gpc}^{-3} \text{ yr}^{-1}$
- Evidence that BBH mass distribution not a simple power law
- Statistical evidence for relativistic orbital precession (and mis-aligned spins)

Potential for studies of redshift evolution, standard siren cosmology, stellar evolution models.

Webinar on 12th November

Population Properties of Compact Objects from the Second LIGO-Virgo Gravitational-Wave Transient Catalog

Preprint: dcc.ligo.org/LIGO-P2000077/public, arXiv: [2010.14533](https://arxiv.org/abs/2010.14533)



Tests of General Relativity

Compact binary coalescence allows us to observe strong gravitational effects that probe GR in strong field, and test GW propagation

- Tighter constraints on Lorentz violation
- Graviton mass $m_g \leq 1.76 \times 10^{-23} \text{ eV}/c^2$
- GW polarisation tests
- ~2x better constraints on post-Newtonian coefficients
- Tests of post-merger object: ringdowns, echoes

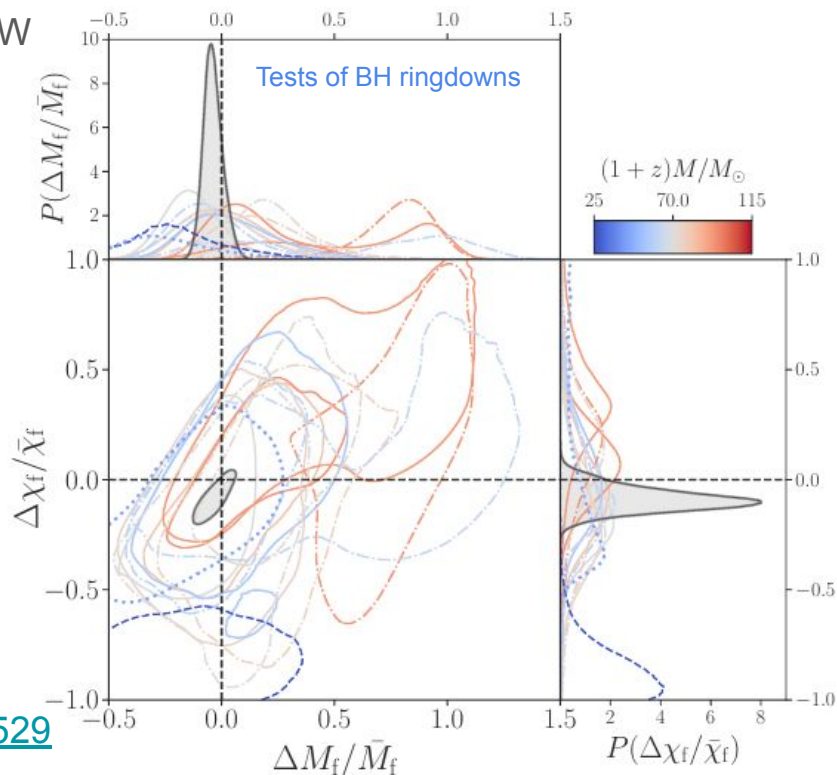
Uses multiple events, and multiple waveform models!

Webinar on 19th November

Tests of General Relativity with Binary Black Holes from the second LIGO–Virgo Gravitational-Wave Transient Catalog

Preprint: dcc.ligo.org/LIGO-P2000091/public arXiv: [2010.14529](https://arxiv.org/abs/2010.14529)

LVC TGR paper, arXiv:[2010.14529](https://arxiv.org/abs/2010.14529)





Data Release

Entire GWTC-2 Transient Catalog available from

www.gw-openscience.org

- Strain data for all events
- Detection statistics (false-alarm-rate)
- Sky localisation maps
- Parameter Estimation Samples for all waveforms

Paper Data Release

- Search sensitivity injection set
- Data behind figures

Available from dcc.ligo.org/LIGO-P2000061/public

→ see referenced documents

Example from Event Portal: GW190707_093326

Documentation

Version: v1

All Versions: v1

GPS: 1246527224.2

UTC Time: 2019-07-07 09:33

Release: GWTC-2

GraceDB: S190707g

GCN: Notices • Circulars

Timeline: Query for segments

DOI: <https://doi.org/10.7935/99gf-ax93>

Data sourced from frame channels.

FrameChannels: [H1:DCS-CALIB_STRAIN_CLEAN_C01, L1:DCS-CALIB_STRAIN_CLEAN_C01]

Data sourced from frame types:

FrameTypes: [H1_HOFT_C01, L1_HOFT_C01]

To open GWF files, use channels names as shown for GWTC-1:
<https://doi.org/10.7935/82H3-HH23>

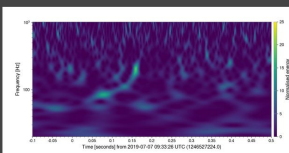
pycbc_highmass Search Pipeline

[show / hide parameters](#)

`far (1/yr)` ≤ 4.6e-05

`network_matched_filter_snr` 12.8

H1 strain



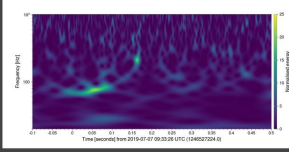
32sec • 16KHz: GWF HDF TXT

32sec • 4KHz: GWF HDF TXT

4096sec • 16KHz: GWF HDF TXT

4096sec • 4KHz: GWF HDF TXT

L1 strain



32sec • 16KHz: GWF HDF TXT

32sec • 4KHz: GWF HDF TXT

4096sec • 16KHz: GWF HDF TXT

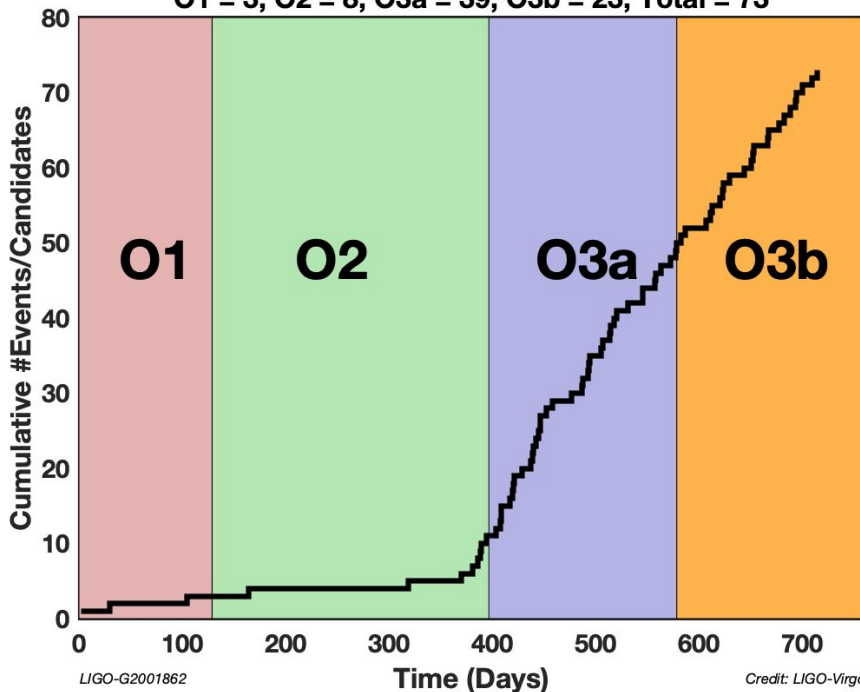
4096sec • 4KHz: GWF HDF TXT



Outlook

Cumulative Count of Events and (non-retracted) Alerts

O1 = 3, O2 = 8, O3a = 39, O3b = 23, Total = 73



O3b

Remainder of O3 [October 2019 - April 2020] still being analysed.

- 23 public alerts released in real-time
- Expanded catalog expected mid-2021

O4

Detectors still under commissioning, some delay (TBD) from covid-19.

KAGRA plans to join O4!

dcc.ligo.org/LIGO-G2001862

Thanks for listening!

Questions?